AJNR

MR imaging of brainstem hemorrhage.

M Komiyama, M Baba, A Hakuba, S Nishimura and Y Inoue

AJNR Am J Neuroradiol 1988, 9 (2) 261-268
http://www.ajnr.org/content/9/2/261

MR Imaging of Brainstem Hemorrhage

Masaki Komiyama[1]
Mitsuru Baba[1]
Akira Hakuba[2]
Shuro Nishimura[2]
Yuichi Inoue[3]

To determine the chronologic changes in the MR appearance of brainstem hemorrhage and to evaluate the clinical efficacy of MR imaging, 15 patients were examined with a 0.5-T MR scanner with inversion-recovery (IR) and T2-weighted spin-echo (SE) images. In the acute stage (up to the sixth day), hematomas were hypo- or isointense on IR images and isointense and then hypointense on SE images. In the subacute stages (the seventh day to 2 months), hematomas changed from hypo- or isointensity to hyperintensity centripetally on IR images and to hyperintensity on SE images. Parenchymal reactions were hypointense first on SE images and then on IR images. In the chronic stage (over 2 months), hematomas "disappeared" and the parenchyma was hypointense on both IR and SE images.

The superior clinical efficacy of MR imaging relative to CT for the detection of hemorrhage was obvious except in the acute stage, when hematomas had an intensity similar to that of the adjacent brainstem, and the patients usually were in serious condition.

MR imaging is accepted as an efficacious diagnostic method, especially for posterior fossa disease, because of its high tissue contrast, lack of artifacts from surrounding bony structures, and wide variety of imaging sequences [1–5]. Intracranial hematomas are of much interest because of their distinctive appearance on MR images. To date, few reports have been published on intracranial hematomas with follow-up periods of over 1 year. We focus on the chronologic changes in the MR appearance of brainstem hemorrhage and discuss the clinical efficacy of MR imaging.

Subjects and Methods

Fifteen patients with brainstem hemorrhages (12 men and three women 43–72 years old) (Table 1) who were diagnosed by CT at the onset of hemorrhage were studied with a 0.5-T cryogenic superconductive MR scanner* with a 30-cm-bore head coil. Time intervals from the onset of brainstem hemorrhage to MR were 5 hr (day 0) to 14 months. Some cases were examined more than once, and MR was performed a total of 36 times. Before MR, the patients primarily had been studied with CT, with the Somatom DR3† and CT/T 8800 and 9000‡ scanners. For MR, T1-weighted inversion-recovery (IR) images were obtained with a repetition time (TR) of 2100–2500 msec, inversion time (TI) of 600 msec, and echo time (TE) of 40 msec (IR 2100–2500/600/40); T2-weighted spin-echo (SE) images were obtained with a TR of 1800–2500 msec and TE of 120 msec (SE 1800–2500/120). Image reconstruction was performed with two-dimensional Fourier transformation. The multiple-slice technique was used. Eight sections, each approximately 1.0-cm thick, were imaged simultaneously in one study. The image matrix was 256^2 and single excitations were used. Most images were in

Received February 10, 1987; accepted after revision August 26, 1987.

[1] Department of Neurosurgery, Baba Memorial Hospital, 244, Higashi 4, Hamadera-Funao-Cho, Sakai, Osaka 592, Japan. Address reprint requests to M. Komiyama.

[2] Department of Neurosurgery, Osaka City University Medical School, 1-5-7, Asahi-machi, Abeno, Osaka 545, Japan.

[3] Department of Radiology, Osaka City University Medical School, Osaka 545, Japan.

AJNR 9:261–268, March/April 1988
0195-6108/88/0902-0261

* Picker International, Highland Heights, OH.
† Siemens Medical Systems, Inc. Iselin, NJ.
‡ General Electric Medical Systems, Milwaukee, WI.

TABLE 1: Intervals from Onset of Brainstem Hemorrhage to MR Examination

Case No.	Age	Gender	Intervals (in Days) from Onset of Hemorrhage (Day 0) to MR
1	72	M	0, 56, 115
2	62	F	1, 8, 19, 52
3	58	F	2, 4, 7, 11, 14, 21
4	57	M	7, 19, 32, 63, 105
5	43	M	9, 15
6	49	M	10
7	58	M	14
8	51	M	20, 102
9	53	M	21
10	53	F	40, 434
11	58	M	43, 67, 170
12	49	M	52, 329, 392
13	61	M	81
14	48	M	168
15	54	M	279

the transverse plane. Cerebral angiography was not performed in any case. Two aspects were evaluated: (1) The intensities of the hematoma and the brain parenchyma immediately adjacent to the hematoma were evaluated with respect to the time interval from the onset of hemorrhage to MR. The hematoma was divided into two parts, central and peripheral. The signal intensities of both parts of the hematoma and of the brain parenchyma were studied independently. (2) The diagnostic efficacy of MR imaging was compared with that of CT for the detection of brainstem hemorrhages.

Results

Chronological changes in MR signal intensity and CT density are shown in Figure 1. The signal intensity of hemorrhage was assessed relative to that of normal white matter on both IR and SE images. The time interval from hemorrhage to MR examination is given, the day of hemorrhage being day 0.

From day 0 to day 1, the entire hematoma was hypo- or isointense on IR images and isointense on SE images (Fig. 2). Then, as early as day 2, the peripheral part of the hematoma became hyperintense on IR images (Fig. 3A) and could remain hypertintense until day 56, while the central part of the hematoma could remain hypointense or isointense as late as day 56. On SE images, the entire hematoma was markedly hypointense from day 2 to day 4 (Fig. 3B).

On IR images, the central part of the hematoma began to be hyperintense as early as day 7 and could remain hyperintense until day 40. Peripheral hyperintensity usually proceeded to central hyperintensity (Figs. 4A, 5A, and 6A). On SE images, the entire hematoma was hyperintense from day 7 to day 67 (Figs. 4B, 5B, and 6B).

Finally, on IR images, the hyperintensity of the hematoma disappeared as early as day 52. On SE images, the hyperintensity of the hematoma disappeared as early as day 63. On IR images, brain parenchyma immediately adjacent to the hematoma began to be of low intensity as early as day 21 (Fig. 7A). The same area began to be of low intensity as early as day 10 on SE images (Fig. 7B). Thereafter, brain parenchyma remained of low intensity on both IR and SE images (Fig. 8).

Small presumed cyst formations were observed on five occasions as early as day 63. Cysts showed intensities similar to that of CSF; that is, low intensity on IR images and high intensity on SE images.

Unenhanced CT was performed at the same time as MR in 31 instances; on six occasions brainstem hemorrhage was of high density as late as day 8. On 10 occasions hematomas could be recognized as vaguely demarcated low-density areas, but on the remaining 15 occasions hematomas could not be identified and CT revealed no abnormalities. Low-density areas appeared as early as day 14. MR imaging was performed a total of 36 times. On all occasions, abnormalities could be identified with MR imaging, regardless of the signal intensity of the hematomas.

Discussion

In early reports, intracranial hematomas were recognized on MR images by their short T1 and long T2 values [2, 6]. However, the relaxation times of hematomas were noted to change during their clinical evolution.

We divided the clinical course of hematomas into three stages: (1) from the onset of hemorrhage to day 6, (2) from day 7 to 2 months, and (3) from 2 months onward (Table 2). In the acute stage (up to day 6), the signal intensity of the hematoma was hypo- or isointense relative to normal white matter on IR images and isointense initially on SE images (days 0–1). The hematoma then became hypointense on SE images (days 2–4) and remained hypointense on IR images, though it began to be hyperintense around the periphery (day 2).

In the subacute stage (day 7 to 2 months), the periphery of the hematomas was hyperintense on IR images, while the central part was hypo- or isointense initially and later became hyperintense. On SE images, the entire hematoma was hyperintense. At the end of the subacute stage, the entire hematoma was hyperintense on both IR and SE images. Brain parenchyma immediately adjacent to the hematoma became hypointense first on SE images and then on IR images.

In the chronic stage (2 months and later), the hematoma signals disappeared as early as day 63 on both IR and SE images. In some cases small presumed cysts were observed that were of low intensity on IR images and of high intensity on SE images. Parenchymal low intensity on both IR and SE images was prominent during this stage.

Many reports have discussed the acute and subacute stages [7–10], but few the chronic stage. Sipponen et al. [7] reported a rather long T1 in acute hemorrhage, with the T1 becoming short at the end of the first week and the signal intensity of the hematoma increasing on IR images up to the second week. Our observations were similar to theirs: The shortening of the T1 of hematoma began at the periphery,

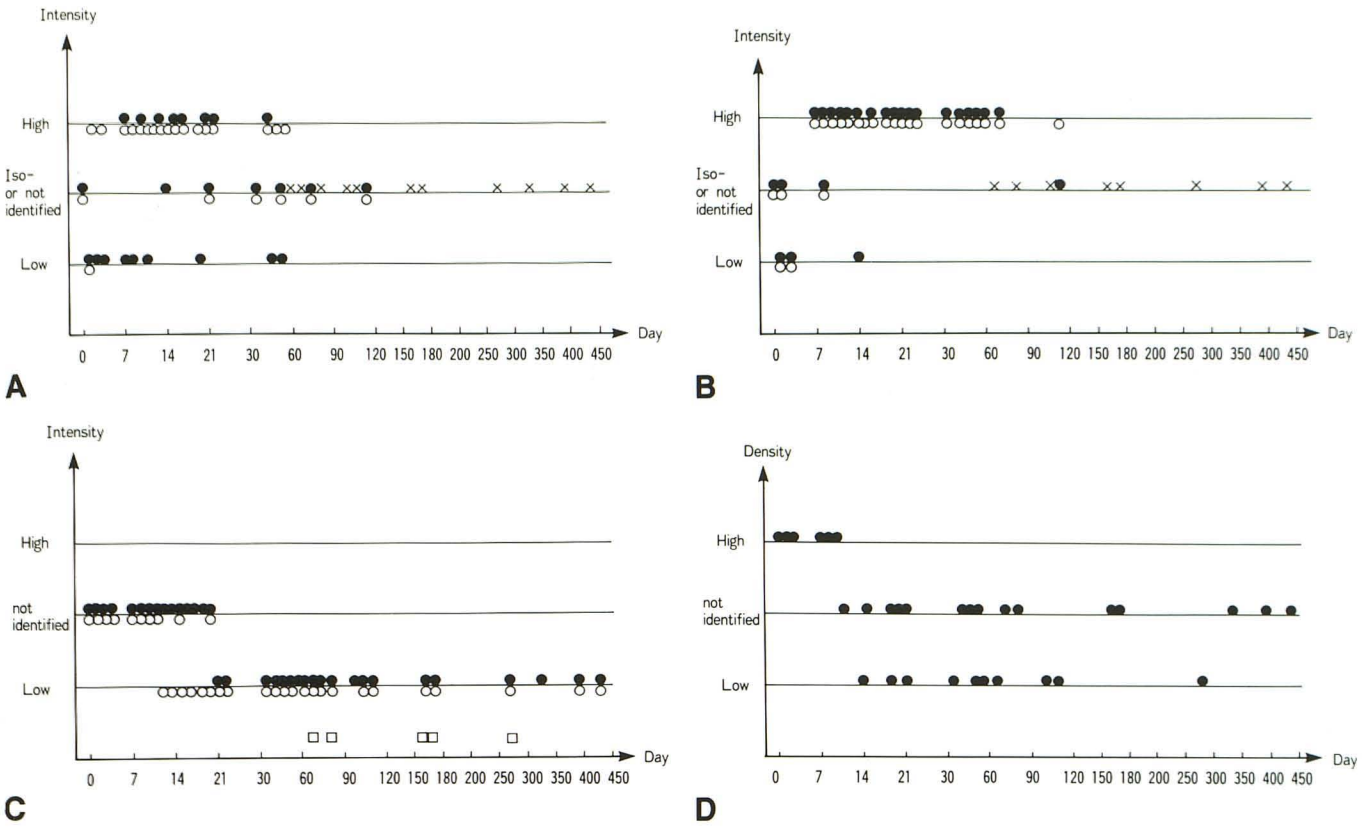

Fig. 1.—Chronologic changes in MR intensities and CT densities from brainstem hemorrhage.
***A* and *B*, Intensities of center (*solid circles*) and periphery (*open circles*) of hematomas on IR (*A*) and SE (*B*) images. X = not identified.**
***C*, Intensities of parenchymal reactions on IR (*solid circles*) and SE (*open circles*) images. Presumed cyst formation (*squares*).**
***D*, CT densities of hematomas.**

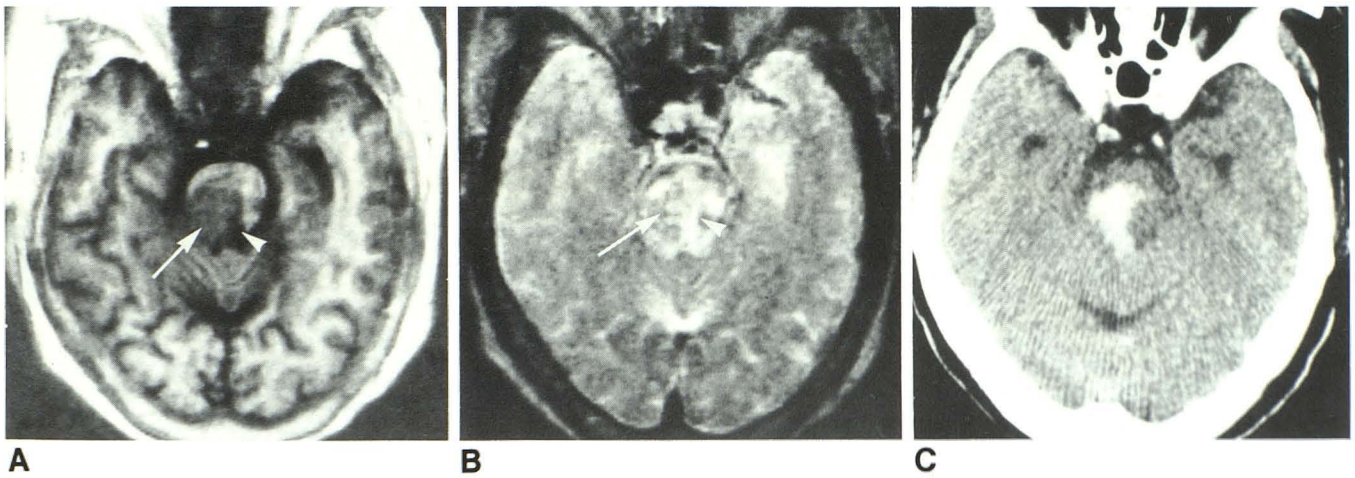

Fig. 2.—Case 2: day 1. IR 2100/600/40 image (*A*), SE 1800/120 image (*B*), and CT scan (*C*). Entire hematoma (*arrows*) is of low intensity on IR and of isointensity on SE images relative to white matter. Surrounding hematoma, very low-intensity area on IR image and high-intensity area on SE image indicate edema (*arrowheads*).

and this high intensity on IR images subsequently filled the entire hematoma. T2 values of a fresh hematoma were short and comparable to those of adjacent brain tissue [9]. DeLaPaz et al. [10] reported that acute hematomas had a relatively short T1 and short T2, which changed to short T1 and long T2. They indicated that the precise turning point was unclear. They did not find that hematoma signals disappeared and parenchymal reaction followed in the chronic stage, which

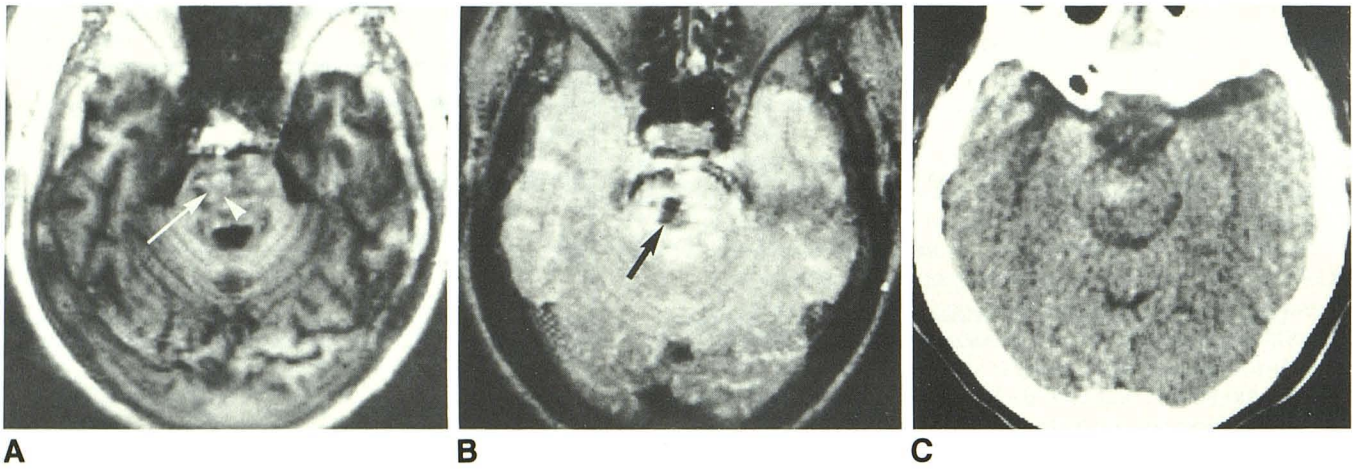

Fig. 3.—Case 3: day 2. IR 2100/600/40 image (*A*), SE 1800/120 image (*B*), and CT scan (*C*). Hematoma is of high intensity at periphery (*arrow*) and of low intensity at center (*arrowhead*) on IR image (*A*). On SE image (*B*), center and periphery of hematoma are of marked low intensity (*arrow*). Edema around hematoma is noted on both IR and SE images.

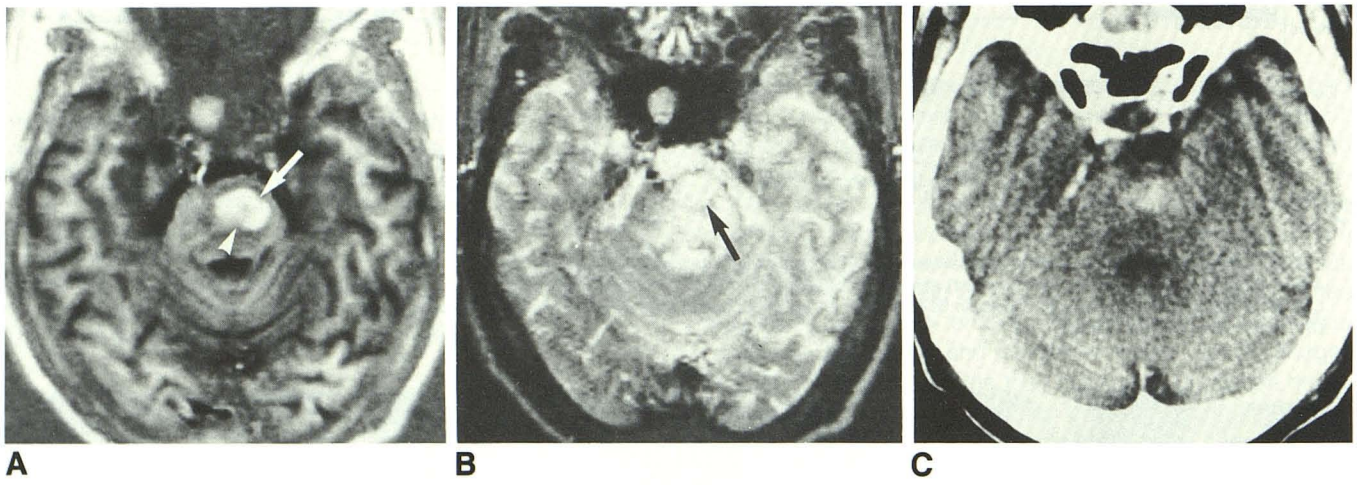

Fig. 4.—Case 4: day 7. IR 2500/600/40 image (*A*), SE 2500/120 image (*B*), and CT scan (*C*). Hematoma is of high intensity at periphery (*arrow*) and of low intensity at center (*arrowhead*) on IR image (*A*), while entire hematoma is of high intensity on SE image (*B*, *arrow*). Hematoma is still high-density area on CT.

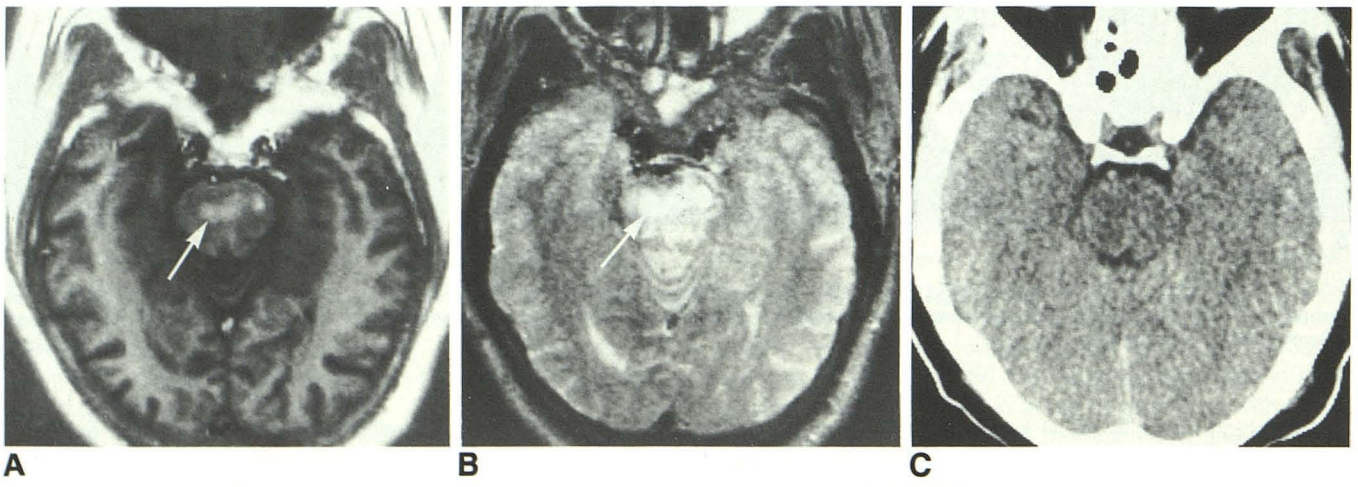

Fig. 5.—Case 5: day 9. IR 2100/600/40 image (*A*), SE 1800/120 image (*B*), and CT scan (*C*). Entire hematoma (*arrows*) is of high intensity on both IR and SE images. Edema around hematoma is seen in both sequences. CT does not show hematoma, but brainstem swelling is suspected.

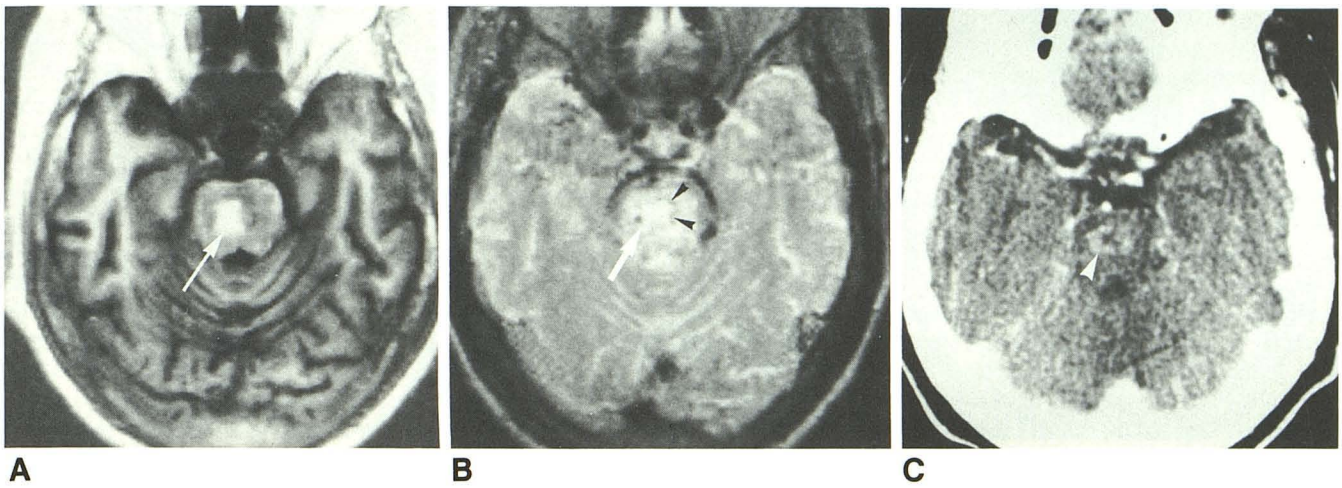

Fig. 6.—Case 3: day 14. IR 2100/600/40 image (*A*), SE 1800/120 image (*B*), and CT scan (*C*). Entire hematoma (*arrows*) is of high intensity on both IR and SE images. On SE image (*B*), brain parenchyma immediately adjacent to hematoma is of low intensity (*arrowheads*). On contrast-enhanced CT scan (*C*), ring enhancement (*arrowhead*) parallels low-intensity area on SE image. Edema is still observed around hematoma in both MR sequences.

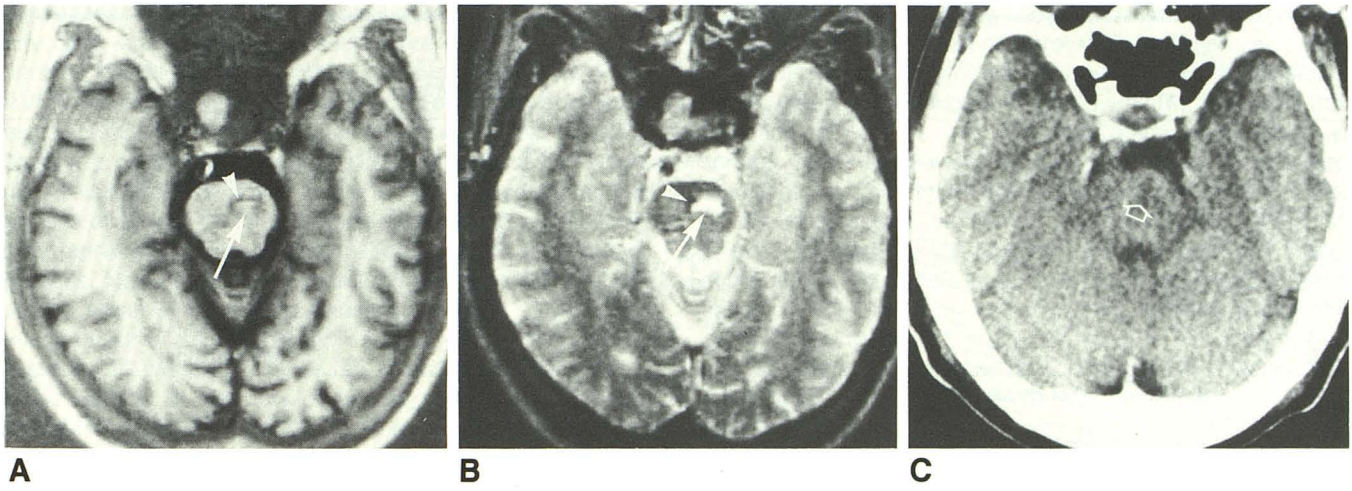

Fig. 7.—Case 4: day 32. IR 2500/600/40 image (*A*), SE 2500/120/image (*B*), and CT scan (*C*). Entire hematoma (*arrows*) is isointense relative to white matter on IR image and highly intense relative to white matter on SE image. Brain parenchyma immediately adjacent to hematoma is of low intensity on both IR and SE images (*arrowheads*). Edema is not observed in either sequence. CT scan has low-density area (*arrow*).

can be expained by their short follow-up period of 42 days. Our observations revealed that the signal intensity of parenchyma adjacent to the hematoma decreased initially on SE images and then on IR images. Although hematoma signals disappeared eventually, parenchymal abnormalities remained and were hypointense on both IR and SE images unless there was cyst, which was hypointense on IR and hyperintense on SE images, simlar to CSF.

Gomori et al. [11] observed (1) a central low intensity on T2-weighted images in the acute stage, (2) a change to high intensity on T1-weighted images and then on T2-weighted images extending from the hematoma periphery inward in the subacute stage, and (3) a rim of parenchymal low intensity abutting the hematoma on T2-weighted images in the subacute and chronic stages. The first and third findings were observed only at high magnetic fields. However, we commonly observed all three findings at intermediate magnetic field strengths (0.5 T).

The peripheral low intensity on T2-weighted SE images in the subacute stage was quite similar to the ring blush after administration of contrast material in CT. On the contrast-enhanced CT scan on day 14 (Fig. 6C) this ring blush was quite similar to the peripheral low intensity on SE images. Zimmerman et al. [12] reported that this ring blush was from gliosis and infiltration with hemosiderin-laden macrophages, and neovascularity was also observed in the granulation tissue around the hematoma. Laster et al. [13] reported that early ring formation was from blood-brain barrier breakdown,

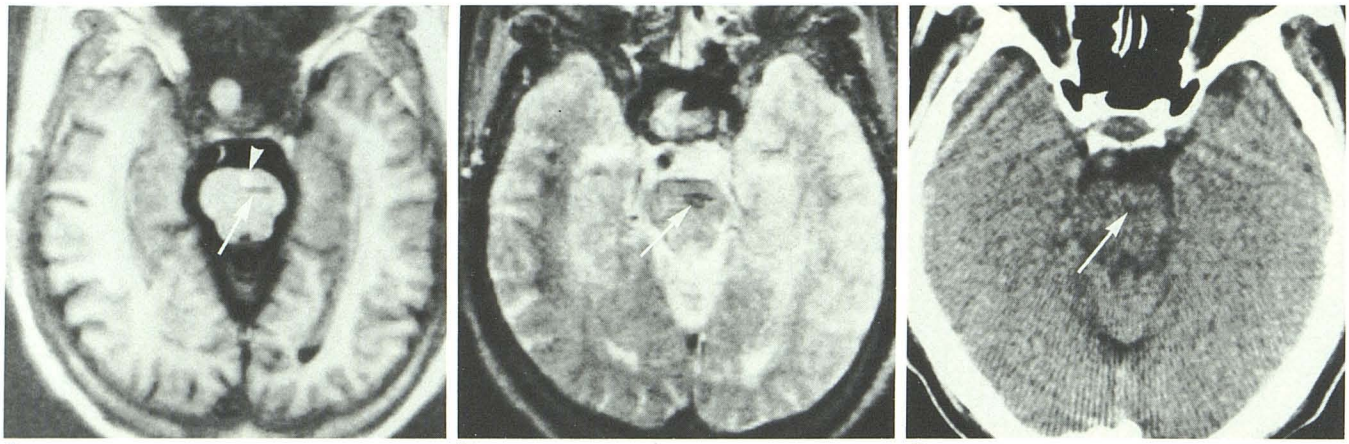

Fig. 8.—Case 4: day 105. IR 2100/600/40 image (*A*), SE 1800/120 image (*B*), and CT scan (*C*). Hematoma signal has disappeared, and parenchymal reaction (*arrows*) is observed as low-density area on both IR and SE images. CT shows low-density area (*arrow*). Edema is not seen on MR images. *Arrowhead* in *A* indicates artifact at center of field of view.

TABLE 2: Changes in MR Signal Intensities During Clinical Stages of Brainstem Hemorrhage

Stage: MR Sequence	Signal Intensity			Hemoglobin Derivatives
	Center of Hematoma	Periphery of Hematoma	Parenchyma	
Acute (≤6 days):				
IR	Low, iso	Low, iso	?	Deoxyhemoglobin
SE[a]	Iso→low	Iso→low	?	Deoxyhemoglobin
Subacute (7 days to 2 months):				
IR	Low, iso→high	High	Low	Methemoglobin
SE[a]	Low→high	High	Low	Methemoglobin
Chronic (≥2 months):				
IR	?[b]	?[b]	Low	Hemosiderin
SE[a]	?[b]	?[b]	Low	Hemosiderin

Note.—iso = isointense; ? = not identified.

[a] T2-weighted.

[b] Presumed cyst formation was noted occasionally.

and late ring formation was from vascular granulation tissue. These observations suggest that hemosiderin is responsible for producing low intensity on IR and SE images in the subacute and chronic stages.

There has been no full explanation for the intensity changes in the evolution of hematoma. In the acute stage, deoxyhemoglobin without cell lysis is believed to be responsible for producing low intensity on T2-weighted images. The mechanism is the preferential T2 proton relaxation enhancement caused by heterogeneity in magnetic susceptibility from deoxyhemoglobin [11]. In the subacute stage, methemoglobin appears and cell lysis occurs. Lysed RBCs are 5% more effective than intact RBCs in shortening T1 values [14]. However, Bradley et al. [15] reported that RBC lysis had no significant effect on T1 and T2 relaxation. High intensities in this stage are believed to correlate with methemoglobin. Di Chiro et al. [16] revealed experimentally that the change in 1/T1 was roughly proportional to the methemoglobin concentration for values up to 40%. In the chronic stage, resorption of methemoglobin occurs and hemosiderin appears. New et al. [17] explained that a decrease in or an absence of SE signal intensity was from the magnetic susceptibility effect of paramagnetic hemosiderin (paramagnetic "clump"). On our IR images, hemosiderin was hypointense. This is not because hemosiderin has long T1 values, but because hemosiderin caused preferential T2 proton relaxation enhancement, and the relatively long TE (40 msec) of our IR sequences introduced a T2 component on IR images. In our series, magnetic susceptibility changes caused by deoxyhemoglobin and hemosiderin could be demonstrated even on intermediate-field MR images. However, high-field MR images are much more sensitive since the preferential T2 proton relaxation enhancement is proportional to the square of the magnitude of the main magnetic field [11]. Edelman et al. [18] reported that a modification of the partial-saturation pulse sequence with gradient echoes permitted the acquisition of highly T1- and

T2-weighted images and was markedly sensitive to magnetic susceptibility changes at intermediate field strengths.

The causes of brainstem hemorrhages are seldom obvious. *Angiographically occult arteriovenous malformation* (AVM) applies to AVMs that do not show abnormal vascularity on cerebral angiography. Since angiography was not performed in any of our cases and there was no histopathologic confirmation of occult AVMs, we have no proof that our MR images show hematoma exclusively, and not also occult AVMs. Angiographically occult AVMs usually appear on plain CT as either homogeneous or mottled, isodense or slightly hyperdense foci 2–3 cm in maximum size that enhance to a minimal or moderate degree with contrast media [19–22].

It is of great interest whether MR can demonstrate angiographically occult AVMs in the brainstem. Kucharczyk et al. [23] reported 13 occult AVMs that appeared on MR as regions of relative signal void in three, hemorrhage in 12, and peripheral edema in seven. Evidence of slow flow (even-echo rephasing) was not observed in any case, and all regions of signal void were attributed to calcification rather than to high-flow vessels. Lemme-Plaghos et al. [24] also reported that flow-related effects such as flow enhancement, high-velocity signal loss, and even-echo rephasing were not observed in any case, and pathologic vessels were not detected. Conversely, Lee et al. [25] reported five angiographically occult AVMs in the brainstem and found multiple areas of decreased signal within the hematoma in all cases, three of which showed a curvilinear decreased signal around the hematoma on T1-weighted SE images. Lee et al. concluded that the regions of absent signal within and surrounding a hematoma may represent vessels of the malformation or a pathologic process. New et al. [17] reported six occult AVMs and observed areas of very low or absent signal on T1-weighted images (four of six cases) and areas of very low or absent signal on T2-weighted images (six of six). They thought that these regions of very low or absent signal were from the magnetic susceptibility effect of hemosiderin and not from vascular flow or calcification.

When we study the MR images of brainstem hemorrhage, we must consider abnormal vessels, calcification, and hemorrhage separately. Hemorrhage has the characteristic MR appearance described above, with changes in signal intensities over time. The signal intensity and shape of abnormal vessels and calcification may not change over time. Low-intensity regions on both IR and T2-weighted SE images may represent rapidly flowing blood in a vascular malformation, hemosiderin in the reactive brain tissues after hemorrhage, or calcification. Furthermore, in the very early stage of hemorrhage (days 2–4), hematomas show marked hypointensity on T2-weighted SE images. Calcification is easily recognized on plain CT scans. In the posterior fossa, however, streak artifacts from the surrounding bone prevent its ready recognition. To differentiate between the flow void of a vascular malformation and hemosiderin, repeated MR studies are of vital importance to avoid the erroneous interpretation of hemosiderin as vascular malformation. Abnormal vessels generally do not change in size and shape, and hemosiderin does not appear in the very early stage of the hemorrhage. Subclinical, recurrent hemorrhage, however, may make this differentiation more complicated, since a fresh hematoma and hemosiderin can coexist. The absence of hemorrhage on MR may be a sensitive indicator that one is dealing with a disease other than an angiographically occult AVM; in particular, a neoplasm. The presence of hemorrhage, on the other hand, is suggestive of, but not specific evidence for an occult AVM [24]. Our results showed that these brainstem lesions exhibited characteristic changes in signal intensities on both IR and T2-weighted SE images, and no calcifications were seen on plain CT in the chronic stage. Most of the patients had a history of hypertension, favoring the diagnosis of primary brainstem hemorrhage. Although there is a possibility that some of the brainstem lesions in our series were hematomas caused by vascular malformations, it is our impression that it is still difficult to differentiate with certainty angiographically occult AVM from primary brainstem hemorrhage, after a relatively large hemorrhage, with the use of MR alone.

As for relative clinical efficacies in the detection of brainstem hemorrhage, MR is superior to CT (except in the acute stage, when hematomas have an intensity similar to that of the adjacent brainstem) because of its high tissue contrast, lack of artifacts from surrounding bony structures, and multiplanar sectioning. Moreover, MR can provide localization and delineation of the extent of the hematoma and show mass effect on adjacent structures better than CT can [5]. However, the condition of patients with brainstem hemorrhage often is serious. Currently, the MR scanning time usually is far longer than that for CT. Current MR imaging systems often have neither satisfactory monitoring nor life-support systems. These facts degrade MR imaging as a diagnostic tool in the acute stage. Thus, MR imaging in the acute stage is less satisfactory than it is later for evaluating patients after intracranial hemorrhage. CT should be used in the acute stage and MR in the subacute and chronic stages [15]. To use MR in the acute stage, especially for the critically ill patient, life-support and monitoring systems have to be developed that can function in a high magnetic field [8].

In conclusion, we divided the clinical course of brainstem hemorrhage into three stages: (1) the acute stage (up to day 6), (2) the subacute stage (day 7 to 2 months), and (3) the chronic stage (2 months and later). In the acute stage, hematomas are hypo- or isointense on IR images and isointense and then hypointense on T2-weighted SE images. In the subacute stage, hematomas change from hypo- or isointensity to hyperintensity centripetally on IR images and to hyperintensity on SE images. In the chronic stage, hematoma signals disappear and parenchymal reaction is hypointense on both IR and SE images. The clinical efficacy of MR in the detection of brainstem hemorrhage is clear, and MR is diagnostically superior to CT except in the acute stage of hemorrhage.

REFERENCES

1. Young IR, Burl M, Clarke GJ, et al. Magnetic resonance properties of hydrogen: imaging the posterior fossa. *AJR* **1981**;137:895–901
2. Bydder GM, Steiner RE, Young IR, et al. Clinical NMR imaging of the brain: 140 cases. *AJNR* **1982**;3:459–480, *AJR* **1982**;139:215–236

3. Bydder GM, Steiner RE, Thomas DJ, Marshall J, Gilderdale DJ, Young IR. Nuclear magnetic resonance imaging of the posterior fossa: 50 cases. *Clin Radiol* **1983**;34:173–188
4. Kistler JP, Buonanno FS, DeWitt LD, Davis KR, Brady TJ, Fisher CM. Vertebral-basilar posterior cerebral territory stroke—delineation by proton nuclear magnetic resonance imaging. *Stroke* **1984**;15:417–426
5. Han JS, Bonstelle CT, Kaufman B, et al. Magnetic resonance imaging in the evaluation of the brainstem. *Radiology* **1984**;150:705–712
6. Bailes DR, Young IR, Thomas DJ, Straughan K, Bydder GM, Steiner RE. NMR imaging of the brain using spin-echo sequences. *Clin Radiol* **1982**;33:395–414
7. Sipponen JT, Sepponen RE, Sivula A. Nuclear magnetic resonance (NMR) imaging of intracerebral hemorrhage in the acute and resolving phases. *J Comput Assist Tomogr* **1983**;7:954–959
8. Zimmerman RA, Bilaniuk LT, Grossman RI, et al. Resistive NMR of intracranial hematomas. *Neuroradiology* **1985**;27:16–20
9. Sipponen JT, Sepponen RE, Tankku JI, Sivula A. Intracranial hematomas studied by MR imaging at 0.17 and 0.02 T. *J Comput Assist Tomogr* **1985**;9:698–704
10. DeLaPaz RL, New PFJ, Buonanno FS, et al. NMR imaging of intracranial hemorrhage. *J Comput Assist Tomogr* **1984**;8:599–607
11. Gomori JM, Grossman RI, Goldberg HI, Zimmerman RA, Bilaniuk LT. Intracranial hematomas: imaging by high-field MR. *Radiology* **1985**;157:87–93
12. Zimmerman RD, Leeds NE, Naidich TP. Ring blush associated with intracerebral hematoma. *Radiology* **1977**;122:707–711
13. Laster DW, Moody DM, Ball MR. Resolving intracerebral hematoma: alteration of the "ring sign" with steroids. *AJR* **1978**;130:935–939
14. Singer JR, Crooks LE. Some magnetic studies of normal and leukemic blood. *J Clin Eng* **1978**;3:237–243
15. Bradley WG, Schmidt PG. Effect of methemoglobin formation on the MR appearance of subarachnoid hemorrhage. *Radiology* **1985**;156:99–103
16. Di Chiro G, Brooks RA, Girton ME, et al. Sequential MR studies of intracerebral hematomas in monkeys. *AJNR* **1986**;7:193–199
17. New PFJ, Ojemann RG, Davis KR, et al. MR and CT of occult vascular malformations of the brain. *AJNR* **1986**;7:771–779
18. Edelman RR, Johnson K, Buxton, et al. MR of hemorrhage: a new approach. *AJNR* **1986**;7:751–756
19. Bell BA, Kendall BE, Symon L. Angiographically occult arteriovenous malformations of the brain. *J Neorol Neurosurg Psychiatry* **1978**;41:1057–1064
20. Becker DH, Townsend JJ, Kramer RA, Newton TH. Occult cerebrovascular malformations. A series of 18 histologically verified cases with negative angiography. *Brain* **1979**;102:249–287
21. Shuey HM Jr, Daly AL, Quisling RG, Sypert GW. Angiographically cryptic cerebrovascular malformations. *Neurosurgery* **1979**;5(4):476–479
22. Hashim ASM, Asakura T, Koichi U, et al. Angiographically occult arteriovenous malformations. *Surg Neurol* **1985**;23:431–439
23. Kucharczyk W, Lemme-Pleghos L, Brant-Zawadzki M, Doom G, Norman D. Intracranial vascular malformations: MR and CT imaging. *Radiology* **1985**;156:383–389
24. Lemme-Plaghos L, Kucharczyk W. Brant-Zawadzki M, et al. MR imaging of angiographically occult vascular malformations. *AJNR* **1986**;7:217–222
25. Lee BCP, Herzberg L, Zimmerman RD, Deck MDF. MR imaging of cerebral vascular malformations. *AJNR* **1985**;6:863–870